An Image Fusion Approach Based on Markov Random Fields

Min Xu, *Member, IEEE*, Hao Chen, *Member, IEEE*, and Pramod K. Varshney, *Fellow, IEEE*

***Abstract*—Markov random field (MRF) models are powerful tools to model image characteristics accurately and have been successfully applied to a large number of image processing applications. This paper investigates the problem of fusion of remote sensing images, e.g., multispectral image fusion, based on MRF models and incorporates the contextual constraints via MRF models into the fusion model. Fusion algorithms under the maximum *a posteriori* criterion are developed to search for solutions. Our algorithm is applicable to both multiscale decomposition (MD)-based image fusion and non-MD-based image fusion. Experimental results are provided to demonstrate the improvement of fusion performance by our algorithms.**

***Index Terms*—Markov random field, multi-resolution decomposition, multispectral image fusion.**

I. Introduction

IMAGE FUSION is important in many image analysis tasks in which image data are acquired from multiple sources. The goal of image fusion is to combine relevant information from two or more source images into one single image such that the single image contains as much information from all the source images as possible. The source images involved in such applications can be taken at different times and/or using different sensors. As a result, some source images may contain certain occlusions and source images from different sensors show different physical features. Thus, the fused image is expected to have a more accurate description of the scene and is, therefore, more useful for human visual or machine perception [1]. In remote sensing applications, there have been a few studies on fusing high-resolution panchromatic images and low-resolution multispectral images to improve the spatial resolution [2], [3]. In this paper, we focus on the fusion of remote sensing images having the same resolution, e.g., multispectral image fusion. A multispectral band covers only a narrow spectral range [3], and different bands represent different aspects of the scene. Multispectral image fusion involves the fusion of several bands in order to improve spectral resolution.

The existing image fusion approaches can be classified into three categories: pixel-level, feature-level, and decision-level [4]. An overview of these image fusion approaches can be found in [4]. This paper is focused on the pixel-level fusion approach. Before image fusion, an image registration algorithm usually needs to be applied in order to align the source images [5]. In this paper, we assume that registered images are available prior to fusion. A variety of image fusion algorithms have been proposed for different applications [6]. The basic pixel-level fusion rule includes two steps.

1) First, we need to determine whether a source image contributes to the fused image for each pixel.
2) Second, the intensity of the pixel in the fused image is obtained from all the contributing source images.

Among the pixel-level fusion rules, two traditional approaches to fusion are to average the pixel intensities from all the source images or take the maximal pixel intensity among all the source images. The averaging approach is effective in removing the Gaussian noise and increases the signal-to-noise ratio (SNR) but makes the image smoother and results in the loss of contrast information. The maximizing approach can produce the fused image at full contrast but is sensitive to sensor noise [7]. To overcome the limitations of the averaging and maximizing approaches, Sharma *et al.* [7] proposed a Bayesian image fusion approach and related it to local principal component analysis.

In recent years, multiscale decomposition (MD)-based techniques have been successfully applied to image fusion for different applications such as concealed weapon detection [8] and hyperspectral image fusion [9]. Different MD methods including pyramid transform and discrete wavelet transform have been applied to image fusion. The performances of these MD-based image fusion approaches are evaluated in [6] for a digital camera application. The MD-based image fusion approaches consist of three steps.

1) The source images are first decomposed into several scale levels using a pyramid transform or a wavelet transform.
2) Fusion is then applied at each level of the source images.
3) Finally, we invert the transform to synthesize the fused image.

The MD-based image fusion approach provides both spatial and frequency domain localization and achieves much better

Manuscript received May 29, 2009; revised June 6, 2010 and February 22, 2011; accepted April 23, 2011. Date of publication July 28, 2011; date of current version November 23, 2011.

M. Xu was with the Department of Electrical Engineering and Computer Science, Syracuse University, Syracuse, NY 13244 USA. She is now with Blue Highway, LLC, Syracuse, NY 13244-4100 USA (e-mail: mxu@blue-highway.com).

H. Chen is with the Department of Electrical and Computer Engineering, Boise State University, Boise, ID 83725-2075 USA (e-mail: haochen@boisestate.edu).

P. K. Varshney is with the Department of Electrical Engineering and Computer Science, Syracuse University, Syracuse, NY 13244 USA (e-mail: varshney@syr.edu).

Color versions of one or more of the figures in this paper are available online at http://ieeexplore.ieee.org.

Digital Object Identifier 10.1109/TGRS.2011.2158607

performance while the use of the transform increases the computational complexity. So one can choose or not to employ transforms on images depending on different applications. For the MD-based fusion approaches, the basic fusion rule is applied to MD representations of the images at each resolution level. For the non-MD-based fusion approach, the basic fusion rule is directly applied to the source images.

Generally, the main drawback of the pixel-level fusion rule is that the decision on whether a source image contributes to the fused image is made pixel by pixel and, therefore, may cause spatial distortion in the fused image, which affects further processing, such as classification and detection. As we know, the pixels in an image are spatially correlated. Thus, for a source image, if one of its pixels contributes to the fused image, its neighbors are also likely to contribute to the fused image. It implies that the decision making during the first step of the fusion process should exploit the property of spatial correlation. Thus, it is important to incorporate spatial correlation into the fusion model, and the use of such a fusion model is expected to improve fusion performance.

A straightforward approach to make use of spatial correlation is to use a window- or region-based method [7], [10]–[13]. The idea is to estimate the intensity of a fused pixel from that of the source images in a small window. Yang and Blum [11] assumed that the decision making of pixels within a small window is constant and developed an expectation-maximization algorithm by employing a Gaussian mixture image model to adaptively find the fusion result. Burt and Kolczynski [10] proposed a weighted average algorithm to estimate the fused image in a pyramid transform domain. The weights are measured based on a local energy or variance (called "salience") within a small window. Lozci *et al.* [12] modified the weighted average algorithm by incorporating a generalized Gaussian statistical model. Lallier and Farooq [13] designed a weighted average scheme for fusing IR and visual images in a surveillance scenario. In their algorithm, larger weights are assigned to either the warmer or cooler pixels for the IR image and to the pixels having larger local variance for the visual image. The aforementioned algorithms [10]–[13] are used in the MD-based fusion approach.

The theory of Markov random fields (MRFs) provides a basis for modeling contextual constraints in visual processing and interpretation [14]. MRF models have proved to be successful in a variety of image processing applications, including multiresolution fusion [15], change detection [16], edge detection [17], image denoising [14], [18], image restoration [19], [20], and image classification [21]. In the image fusion application, an MRF model has been used to model the images for the fusion of edge information [22]. Yang and Blum proposed a statistical model to describe the fusion process [1], [11], [23]. However, the application of MRF models for pixel-level image fusion on images with the same resolution has not been considered. In this paper, we propose two fusion algorithms by incorporating the contextual constraints via MRF models into the fusion model. The first algorithm models the decision making at the first step of the fusion rule as an MRF, and the second algorithm models both the decision making and the true image as MRFs. Also, the first algorithm is applicable for both the MD-based fusion approach and the non-MD-based fusion approach while the second algorithm is only applicable for the non-MD-based fusion approach.

This paper is organized as follows. In Section II, we formulate the image fusion problem based on a statistical model. Then, the MRF-based image fusion approach is presented in Section III. In Section IV, we compare our proposed fusion approach with other fusion approaches via two experiments. Finally, some concluding remarks are provided in Section V.

II. Problem Formulation

Image fusion is essentially an estimation problem. The objective is to estimate the underlying scene, assuming that each source image contains a good view of only part of the scene [1]. Blum [1] has proposed a statistical model for the image fusion problem. Assume that there are N source images to fuse. Each source image can be modeled as

$$y_i(\mathbf{r}) = H_i(\mathbf{r})\, x(\mathbf{r}) + w_i(\mathbf{r}), \qquad i = 1, \ldots, N \tag{1}$$

where $\mathbf{r}$ indicates the spatial coordinates of a pixel, $y_i(\mathbf{r})$ is the intensity of the ith source image at $\mathbf{r}$, $x(\mathbf{r})$ is the intensity of the true scene at $\mathbf{r}$ to be estimated, $w_i(\mathbf{r})$ is the noise, and $H_i(\mathbf{r})$ is the sensor selectivity coefficient, taking on values from $\Theta = \{q_1, q_2, \ldots\}$ representing the percentage of the true scene contributing to the ith source image [7]. In our work, we use $\Theta = \{0, 1\}$, which determines if the true scene contributes to the ith source image or not [1]. In the following, for simplicity of notation, "$(\mathbf{r})$" is omitted.

Note that (1) represents the relationship between the source images and the true scene. According to this model, if the true scene contributes to the source image, the source image is modeled as a true scene plus a Gaussian noise. If the true scene does not contribute to the source image, the source image is modeled as Gaussian noise. In practice, particularly in multiple-sensor applications and multifocus applications, this model has some limitations. The source images obtained from different sensors sense different aspects of the true scene, and this model may be a coarse approximation in this case.

The image fusion problem essentially involves the estimation of H_i and x. The two traditional algorithms, namely, the averaging and maximizing algorithms, can also be expressed using this model. For the averaging algorithm, $H_i = 1$ *for all* i. For the maximizing algorithm, $H_i = 1, i = \max_i\{y_i\}$; $H_i = 0$, *otherwise*.

When H_i is given, the pixel intensity of the fused image can be easily calculated by a Least Squares (LS) technique as [24]

$$\hat{x} = (H^{\mathrm{T}}H)^{-1}H^{\mathrm{T}}Y \tag{2}$$

where H denotes the vector $[H_1, H_2, \ldots, H_N]^{\mathrm{T}}$ and Y denotes the vector $[y_1, y_2, \ldots, y_N]^{\mathrm{T}}$.

In practice, we only have the source images available without any prior information and the coefficient H is usually unknown. According to the LS technique, from the set of all possible

values that the coefficient H can take, the one which produces the highest energy should be selected, i.e.,

$$\begin{aligned}\hat{H} &= \min_{H}\left\{(Y-H\hat{x})^{\mathrm{T}}(Y-H\hat{x})\right\}\\ &= \min_{H}\left\{Y^{\mathrm{T}}Y-(Y^{\mathrm{T}}H)(H^{\mathrm{T}}H)^{-1}(H^{\mathrm{T}}Y)\right\}\\ &= \max_{H}\left\{(Y^{\mathrm{T}}H)(H^{\mathrm{T}}H)^{-1}(H^{\mathrm{T}}Y)\right\}. \end{aligned} \tag{3}$$

Note, since $H_i \in \{0,1\}$, H has 2^N possible values. Once H is available, the intensity of the fused image at pixel $\mathbf{r}$, i.e., x, is obtained by an LS approach [24], which is

$$\hat{x} = (\hat{H}^{\mathrm{T}}\hat{H})^{-1}\hat{H}^{\mathrm{T}}Y. \tag{4}$$

In the aforementioned model, both the coefficient H and the intensity of the fused image x at each pixel are estimated pixel by pixel, and therefore, it is very sensitive to sensor noise. Furthermore, since the estimation of the fused image is based on the estimation of the coefficients, the estimation of the coefficient H plays an important role in the fusion process. The estimation accuracy of the coefficients directly influences the estimation of the fused image. Since the coefficient H of a pixel is likely to be similar to the coefficients corresponding to other pixels in its neighborhood due to spatial correlation, we can get better estimates of H by utilizing spatial correlation.

A straightforward and simple approach is to assume that the coefficients of pixels within a small window are constant and then select the coefficient which produces the highest energy of pixels within a small window. This strategy has been used in [11]. However, the goal of the LS approach is to minimize the data error $\|y-\hat{y}\|^2$, which does not necessarily lead to a small estimation error for either H or x. A popular strategy for improving the estimation error of LS is to incorporate prior information on H or x [25]. Motivated by this fact and the fact that the MRF model in the form of prior Gibbs distributions is currently the most effective way to describe the local behavior of both the intensity field and the discontinuity field [20], we propose to employ an MRF model to estimate the coefficients. It is expected to improve the estimation accuracy of the coefficients H, thereby leading to improved fusion results. In the next section, we develop our image fusion approaches based on MRF modeling.

III. Proposed Algorithms

The image fusion problem is to estimate the true scene x. However, before the estimation of x, we need to obtain an accurate estimate of H, which represents the decision whether the true scene is present in the source image, i.e., whether the source image contributes to the fused image. In the previous section, we considered the estimation of x and H on a pixel level. In this section, we propose two MRF-based image fusion approaches, which design the estimator by incorporating the spatial correlation through the prior probability density function (pdf) of H and x. The intensity of a fused pixel then depends not only on the intensities of the pixel in the source images but also on that of the neighboring pixels. In the first algorithm, only the coefficients are modeled using an MRF, denoted as MRF_H. In the second algorithm, both the coefficients and the fused image are modeled using MRFs, denoted as MRF_HX. Some notations used in the remainder of this paper are listed as follows:

- $\mathbf{X}$: the whole true scene (fused image);
- $\mathbf{H_i}$: the coefficients of the ith source image;
- $\mathbf{Y_i}$: the intensities of the ith source image;
- $\mathbf{H}$: the coefficients of source images, where $\mathbf{H}(\mathbf{r},\mathbf{i}) = \mathbf{H_i}$;
- $\mathbf{Y}$: the intensities of source images, where $\mathbf{Y}(\mathbf{r},\mathbf{i}) = \mathbf{Y_i}$.

The maximum *a posteriori* (MAP) criterion is used to find the optimal solution for the estimation problem. The estimation procedure based on the MAP criterion chooses the most likely values of coefficients and the fused image among all possible values given the observed source images. The resulting probability of error is minimal among all other detectors [24]. This criterion is expressed as

$$\{\hat{\mathbf{H}},\ \hat{\mathbf{X}}\} = \arg\left\{\max_{\mathbf{H},\mathbf{X}}\left[P(\mathbf{X},\mathbf{H}|\mathbf{Y})\right]\right\}. \tag{5}$$

However, due to high computational complexity, it is difficult to directly obtain the final solution. Note that $P(\mathbf{X},\mathbf{H}|\mathbf{Y}) = P(\mathbf{X}|\mathbf{H},\mathbf{Y})P(\mathbf{H}|\mathbf{Y}) = P(\mathbf{H}|\mathbf{X},\mathbf{Y})P(\mathbf{X}|\mathbf{Y})$. Thus, a suboptimal method is adopted in this paper. We decompose our problem (5) into two subproblems and iteratively solve the two subproblems

$$\begin{aligned}\hat{\mathbf{H}}^{n+1} &= \arg\left\{\max_{\mathbf{H}}\left[P(\mathbf{H}|\mathbf{Y},\hat{\mathbf{X}}^n)\right]\right\}\\ \hat{\mathbf{X}}^{n+1} &= \arg\left\{\max_{\mathbf{X}}\left[P(\mathbf{X}|\mathbf{Y},\hat{\mathbf{H}}^n)\right]\right\}\end{aligned} \tag{6}$$

where $\hat{\mathbf{H}}^n$ denotes the nth update of the estimate of $\mathbf{H}$ and $\hat{\mathbf{X}}^n$ denotes the nth update of the estimate of $\mathbf{X}$. It is easy to show that we can iteratively update the estimates of $\mathbf{H}$ and $\mathbf{X}$ such that

$$P(\mathbf{X}^{n+1},\mathbf{H}^{n+1}|\mathbf{Y}) \geq P(\mathbf{X}^n,\mathbf{H}^n|\mathbf{Y}) \tag{7}$$

and, therefore, achieve the optimum at the end.

A. Fusion Approach: MRF Modeling for Coefficients H (MRF_H)

Motivated by the fact that the coefficients of the source images exhibit spatial correlation, we model the coefficient $\mathbf{H}$ by an MRF model. Let S be a set of sites in an image and $\Lambda \in \{0,1,\ldots,L-1\}$ be the phase space. We assume that the coefficients $\mathbf{H}(S) \in \Lambda^S$ follow MRF properties with the Gibbs potential $U_c(\mathbf{H})$. The marginal pdf for $\mathbf{H}$ is written as [14]

$$P_{\mathbf{H}}(\mathbf{H}) = \frac{1}{Z_{\mathbf{H}}}\exp\left[-\frac{1}{T}\sum_{c\subset S}U_c(\mathbf{H})\right] \tag{8}$$

where $Z_{\mathbf{H}}$ is a normalization constant given by

$$Z_{\mathbf{H}} = \sum_{\mathbf{H}\in\Lambda^S}\exp\left[-\frac{1}{T}\sum_{c\subset S}U_c(\mathbf{H})\right]. \tag{9}$$

The estimate of $\mathbf{H}$ is given by

$$\hat{\mathbf{H}}^{n+1} = \arg\left\{\max_{\mathbf{H}}\left[P(\mathbf{H}|\mathbf{Y}, \hat{\mathbf{X}}^n)\right]\right\}. \tag{10}$$

We apply Bayes' rule, which provides the following result:

$$P(\mathbf{H}|\mathbf{Y}, \hat{\mathbf{X}}^n) = \frac{P(\mathbf{H}, \mathbf{Y}|\hat{\mathbf{X}}^n)}{P(\mathbf{Y}|\hat{\mathbf{X}}^n)} = \frac{P(\mathbf{Y}|\mathbf{H}, \hat{\mathbf{X}}^n)P(\mathbf{H})}{P(\mathbf{Y}|\hat{\mathbf{X}}^n)} \tag{11}$$

and because $P(\mathbf{Y}|\hat{\mathbf{X}})$ is constant for all the values of $\mathbf{H}$, (10) can be rewritten as

$$\hat{\mathbf{H}}^{n+1} = \arg\left\{\max_{\mathbf{H}}\left[P(\mathbf{Y}|\mathbf{H}, \hat{\mathbf{X}}^n)P(\mathbf{H})\right]\right\}. \tag{12}$$

In the model given in (1), the noise of each source pixel is assumed to be an independent and identically distributed (i.i.d.) Gaussian noise with zero mean and variance of σ^2, and therefore, the conditional pdf of the source image $\mathbf{Y}$ given $\mathbf{H}$ and $\hat{\mathbf{X}}^n$ is given by

$$P(\mathbf{Y}|\mathbf{H}, \hat{\mathbf{X}}^n) = \frac{\exp\left[-\frac{\sum_i (\mathbf{Y}_i - \mathbf{H}_i\hat{\mathbf{X}}^n)^{\mathrm{T}}(\mathbf{Y}_i - \mathbf{H}_i\hat{\mathbf{X}}^n)}{2\sigma^2}\right]}{(2\pi\sigma^2)^{\frac{M}{2}}} \tag{13}$$

where M is the total number of pixels.

Then, substituting (8) and (13) into (12) and taking the constant term out, we obtain

$$\hat{\mathbf{H}}^{n+1} = \arg\left\{\max_{\mathbf{H}}\left[\exp\left(-E(\mathbf{H})\right)\right]\right\} \tag{14}$$

where

$$E(\mathbf{H}) = \frac{\sum_i (\mathbf{Y}_i - \mathbf{H}_i\hat{\mathbf{X}}^n)^{\mathrm{T}}(\mathbf{Y}_i - \mathbf{H}_i\hat{\mathbf{X}}^n)}{2\sigma^2} + \sum_{c\subset S} U_c(\mathbf{H}). \tag{15}$$

According to the aforementioned result, we observe that maximization in (14) is equivalent to minimization of $E(\mathbf{H})$. Thus, the optimal estimate for $\mathbf{H}$ can be expressed as

$$\hat{\mathbf{H}}^{n+1} = \arg\left\{\min_{\mathbf{H}}\left(E(\mathbf{H})\right)\right\}. \tag{16}$$

Note that, for two source images with size $300 * 300$, $\mathbf{H}$ has a total of 4^{90000} possible configurations. Thus, in practice, due to the large search space on $\mathbf{H}$, the solution of (16) cannot be obtained directly, and therefore, the simulated annealing (SA) algorithm [26] is applied here to search for the optimal solution of (16). The solution for the second subproblem, i.e., the estimate for $\mathbf{X}$, is obtained by (4). The iterative algorithm is described in terms of the following steps.

1) Start with an initial estimate of $\mathbf{H}$ and $\mathbf{X}$. Estimate the initial parameters (noise variance and some parameters in the pdf of $\mathbf{H}$) and set the initial temperature.
2) At each iteration, obtain a new estimate of $\mathbf{H}$ based on the Gibbs pdf given in (8) with the Gibbs potential $E(H)$ using a Gibbs sampling procedure [14].
3) Update the fused image using (4).
4) Reduce the temperature using a predetermined schedule and repeat 2) and 3) until convergence.

Here, the temperature is a parameter which is used to control the randomness of the coefficient generator, and we consider that the algorithm converges when the two consecutive updates are within tolerance of each other. At steps 2) and 3), we visit each pixel from left to right and from top to bottom when we update the coefficients and the fused image. Eventually, the resulting coefficient will converge to the solution of (16), and the fused image is simultaneously obtained. Compared with the maximizing approach, the averaging approach, and the LS approach, the solution of this algorithm is obtained through an optimization algorithm, and therefore, it increases the computation time. However, the MRF modeling of the coefficient in the image model is a better model to describe the fusion process, which improves the fusion performance.

In recent years, other optimization algorithms such as the graph-cut-based approach [27] have become very popular, and they can find the solution in a more computationally efficient manner than the SA optimization algorithm. The use of optimization algorithms such as the graph-cut-based optimization approach will be investigated in the future to improve the efficiency of the fusion algorithm.

Assume that we have N source images of size M. Since the coefficient $H_i(\mathbf{r})$ of the ith source image at pixel $\mathbf{r}$ is taken from $\{0, 1\}$, each component of $\mathbf{H}$ belongs to a set with the size 2^N. Thus, during each iteration, the algorithm to estimate the coefficient has the computational complexity $O(M * 2^N)$ during each iteration.

B. Fusion Approach: MRF Modeling for Coefficients H and Fused Image X (MRF_HX)

In the aforementioned algorithm, we assumed that the coefficients $\mathbf{H}$ follow an MRF model. Then, the intensity of the fused pixel is estimated by an LS technique. In practice, the fused image also has the property of high spatial correlation. Thus, one may assume that the fused image also follows an MRF model with a Gibbs potential $V_c(\mathbf{X})$. Hence, the marginal pdf for $\mathbf{X}$ is written as [14]

$$P_{\mathbf{X}}(\mathbf{X}) = \frac{1}{Z_{\mathbf{X}}}\exp\left[-\frac{1}{T}\sum_{c\subset S} V_c(\mathbf{X})\right] \tag{17}$$

where $Z_{\mathbf{X}}$ is a normalization constant given by

$$Z_{\mathbf{X}} = \sum_{\mathbf{X}}\exp\left[-\frac{1}{T}\sum_{c\subset S} V_c(\mathbf{X})\right]. \tag{18}$$

Under this assumption, the MAP criterion to obtain the optimal $\mathbf{X}$ is written as

$$\hat{\mathbf{X}}^{n+1} = \arg\left\{\max_{\mathbf{X}}\left[P(\mathbf{X}|\mathbf{Y}, \hat{\mathbf{H}}^n)\right]\right\}. \tag{19}$$

In a similar manner as for the estimation of $\hat{\mathbf{H}}$, (19) reduces to

$$\hat{\mathbf{X}}^{n+1} = \arg\left\{\min_{\mathbf{X}}\left(\Delta(\mathbf{X})\right)\right\} \tag{20}$$

where

$$\Delta(\mathbf{X}) = \frac{1}{2\sigma^2}\sum_i \left(\mathbf{Y}_i - \hat{\mathbf{H}}_i^n \mathbf{X}\right)^{\mathrm{T}} \left(\mathbf{Y}_i - \hat{\mathbf{H}}_i^n \mathbf{X}\right) + \sum_{c\subset S} V_c(\mathbf{X}). \tag{21}$$

In the next section, we will show that the solution of (20) can be easily obtained when we use a Gaussian MRF to model the fused image.

Different from the first algorithm MRF_H, where the fused image $\mathbf{X}$ is updated by an LS technique, this new algorithm uses a MAP solution to update the fused image $\mathbf{X}$ using (20). The whole procedure is then described as follows.

1) Start with an initial estimate of $\mathbf{H}$ and $\mathbf{X}$. Estimate the initial parameters (noise variance and some parameters in the pdf of $\mathbf{H}$ and $\mathbf{X}$) and set the initial temperature.
2) At each iteration, obtain a new estimate of $\mathbf{H}$ based on its Gibbs pdf given in (8) with the Gibbs potential $E(H)$ using a Gibbs sampling procedure [14].
3) Update the fused image using the solution of (20).
4) Reduce the temperature using a predetermined schedule and repeat 2) and 3) until convergence.

In summary, it is an iterative estimation process to estimate both $\mathbf{H}$ and $\mathbf{X}$, which increases computational time. The MRF modeling of both the coefficient and the fused image more accurately represents the images with high resolution and therefore produces better fusion results for the fusion of source images with high resolution. Moreover, the initial estimates of $\mathbf{H}$ and $\mathbf{X}$ are important. As the initial estimates of $\mathbf{H}$ and $\mathbf{X}$ get closer to the optimal values, the algorithm converges faster. Poor initial estimates may lead to the local maxima of the *a posteriori* probability. Although the LS approach given by (3) and (4) is found to be a simple and effective fusion approach, it does not take spatial correlation into account. However, we use it to obtain our initial estimates of $\mathbf{H}$ and $\mathbf{X}$. According to our experiments, this approach displays a good fusion performance.

C. Extension to the MD-Based Fusion Framework

Here, the applicability of the two proposed algorithms to the MD-based fusion approach is discussed. For the non-MD-based fusion approach, $\mathbf{Y}$ and $\mathbf{H}$ in the data model (1) denote the intensities of the source images and their corresponding coefficients and $\mathbf{X}$ denotes the intensity of the fused image. This data model (1) is also applicable for the data after the MD process [1], [7]. Thus, if the MD-based fusion approach is employed, we assume that the MD transform is applied to the source images, $\mathbf{Y}$ refers to the values of the MD representations of the source images at some resolution level, $\mathbf{H}$ refers to the corresponding coefficients, and $\mathbf{X}$ refers to the values of the MD representations of the fused image at the same resolution level. Thus, instead of directly applying the image fusion model (1) on the source images, one can perform the MD on the source images and then apply the image fusion model (1) on the MD representations at each resolution level. By using multiresolution transforms such as discrete wavelet transform, the source image is decomposed into different frequency bands, which makes the model (1) more closely fit the MD representations. However, the use of multiresolution transforms increases the complexity of the algorithm. It is noted that, since the multiresolution transform may result in the loss of locality in MRF models for the MD image representations [28], i.e., the local MRF property may not hold on $\mathbf{X}$, it is not suggested to use the algorithm MRF_HX with the MD-based fusion approach.

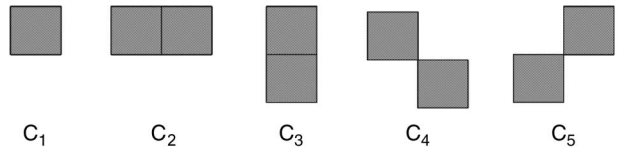

Fig. 1. Cliques considered in the eight-neighborhood system.

The coefficient $\mathbf{H}$ for each pixel represents whether the true scene $\mathbf{X}$ (fused image) contributes to the source image. Pixels in a large area may all contribute to the true scene; however, all the pixels in the area may not contain the same intensities. Thus, the coefficient $\mathbf{H}$ has more spatial correlation over a larger area than the intensity of the true scene $\mathbf{X}$. After MD transformation, coefficients $\mathbf{H}$ may still exhibit spatial correlation while MRF property may not hold for $\mathbf{X}$. Thus, only the algorithm MRF_H is applied in the MD-based fusion approach. In the next section, some examples are provided for illustration.

IV. Experimental Results

A. Choice of MRF Models

We provide three examples to evaluate the fusion performance of our fusion algorithms. For the two MRF-based fusion algorithms, MRF_H and MRF_HX, used in the following experiments, we consider five clique types in the eight-neighborhood system: C_1, C_2, C_3, C_4, C_5, associated with the singleton, vertical pairs, horizontal pairs, left-diagonal pairs, and right-diagonal pairs, respectively. They are shown in Fig. 1. The Gibbs energy function of the coefficient of the source image is defined by an autologistic function, given by [14]

$$\sum_{c\subset S} U_c(\mathbf{H}) = \mathbf{a}^{\mathrm{T}}\mathbf{L} \tag{22}$$

where $\mathbf{a} = [a_2, \ldots, a_5]$ is the parameter vector of the coefficient $\mathbf{H}$ and

$$\mathbf{L} = \left[\sum_{(s,t)\in C_2} I\left[\mathbf{H}(s), \mathbf{H}(t)\right], \ldots, \sum_{(s,t)\in C_5} I\left[\mathbf{H}(s), \mathbf{H}(t)\right]\right] \tag{23}$$

is the coefficient potential vector associated with clique types. Here, the function I is defined as

$$\begin{aligned} I(a,b) &= -1, \quad if\ a = b \\ I(a,b) &= 1, \quad otherwise. \end{aligned} \tag{24}$$

Due to its simplicity, this class of MRF model has been extensively used in [14], [29]–[31] for modeling a wide variety of images, both as region formation models and as texture models.

Furthermore, we use a Gaussian MRF model to represent the Gibbs energy function of the fused image, which is given by

$$\sum_{c\subset S} V_c(\mathbf{X}) = \frac{1}{2}\left(\mathbf{X}(s) - \mathbf{p}^{\mathrm{T}}\mathbf{G}\right)^2 \tag{25}$$

where $\mathbf{p} = [p_2, \ldots, p_5]$ is the parameter vector of the image model and its potential vector $\mathbf{G}$ is defined as

$$\mathbf{G} = \left[\sum_{(s,t)\in C_2} \mathbf{X}(t), \ldots, \sum_{(s,t)\in C_5} \mathbf{X}(t)\right]. \tag{26}$$

For simplicity, we choose $\mathbf{p} = [0.333, 0.333, 0.1667, 0.1667]$ in our experiments. The Gaussian MRF model is widely used for modeling image texture [14]. Under this model, the analytical solution for (20) can be easily derived by

$$\frac{\partial \Delta(\mathbf{X})}{\partial \mathbf{X}} = 0. \tag{27}$$

Substituting (13) and (25) into (27), it yields

$$\hat{\mathbf{X}}^{n+1} = \left(1 + \sum_i \mathbf{H}_i^{n\mathrm{T}}\mathbf{H}_i^n/\sigma^2\right)^{-1}\left(\mathbf{p}^{\mathrm{T}}\mathbf{G} + \sum_i \mathbf{H}_i^{n\mathrm{T}}\mathbf{Y}_i/\sigma^2\right). \tag{28}$$

The estimate given by (28) for one pixel involves vector multiplication, which has the computational complexity $O(N)$. Thus, the estimation of the whole fused image has the computational complexity $O(M * N)$. Because the estimation of the coefficient also has the computational complexity $O(M * 2^N)$ at each iteration, the overall complexity is $O(M * (2^N + N)) \approx O(M * 2^N)$.

B. Parameter Estimation

Modeling the Markov pdf parametrically involves the data-driven optimal estimation of the parameters associated with the potential functions V_c. The model parameters must be estimated for each data set as part of the image processing algorithm. In our algorithms, the noise variance σ^2 in (13) and the parameter $\mathbf{a}$ in the coefficient MRF pdf in (22) are unknown. Thus, we need to estimate these parameters in our algorithms.

Because we assume that the noise in the fusion model is a Gaussian noise, it is straightforward to estimate the noise variance by the maximum likelihood (ML) criterion. It is given by

$$\begin{aligned}\hat{\sigma}^2 &= \arg\max P(\mathbf{Y}|\mathbf{H}, \mathbf{X}, \sigma^2) \\ &= \frac{1}{MN}\sum_i (\mathbf{Y}_i - \mathbf{H}_i\mathbf{X})^{\mathrm{T}}(\mathbf{Y}_i - \mathbf{H}_i\mathbf{X}).\end{aligned} \tag{29}$$

The direct ML estimation of the parameters associated with the pdf of $\mathbf{H}$ is known to be a difficult problem [32]. The ML estimate of $\mathbf{a}$ is

$$\begin{aligned}\hat{\mathbf{a}} &= \arg\max_{\mathbf{a}} P(\mathbf{H}, \mathbf{a}) \\ &= \arg\min_{\mathbf{a}} V_c(\mathbf{H}, \mathbf{a}) - \ln Z_{\mathbf{H}}.\end{aligned} \tag{30}$$

(a) (b) (c)

Fig. 2. Synthetic source images in Experiment 1, size $150 * 150$. (a) Source 1. (b) Source 2. (c) Source 3.

The potential function $V_c(\mathbf{H}, \mathbf{a})$ can be simply computed. However, the normalization term $Z_{\mathbf{H}}$ involves a summation over all possible configurations of $\mathbf{H}$, which is practically impossible due to the large computation time. Note that, for two source images with size $300 * 300$, $\mathbf{H}$ has a total of 4^{90000} possible configurations.

An alternative method for approximation to ML estimation is maximum pseudolikelihood (MPL) estimation, which was proposed by Besag [33]. The MPL estimation method is a suboptimal method, which is given by

$$\begin{aligned}\hat{\mathbf{a}} &= \arg\max_{\mathbf{a}} \prod_s P\left(\mathbf{H}(s), \mathbf{a}\right) \\ &= \arg\min_{\mathbf{a}} \sum_s V_c\left(\mathbf{H}(s), \mathbf{a}\right) - \ln Z_{\mathbf{H}(s)}.\end{aligned} \tag{31}$$

Since each site is not independent of each other, the resulting function is not the true likelihood function. However, Geman and Graffigne [34] later proved that the MPL estimate converges asymptotically to the true ML estimate. Thus, we used this method to estimate the parameters associated with the MRF pdf in our algorithm. To obtain the optimal solution that maximizes the pseudolikelihood, we adopt the Metropolis optimization method [31]. Because parameter estimates do not change appreciably between successive iterations, we update the parameters using this strategy after every ten iterations for $\mathbf{H}$, as suggested in [26].

C. Application With Non-MD-Based Fusion

1) Experiment 1—Synthetic Data: We first implement our two proposed fusion algorithms, MRF_H and MRF_HX, for non-MD-based fusion approaches. In this experiment, we generated three source images based on the model given in (1), as shown in Fig. 2. The image "Campus" of size $150 * 150$ is used as our original image. For each source image, we generated the coefficient mask H_i by a Gibbs sampling generator. The value 0 of the coefficient represents occlusion in the source image, and the value 1 of the coefficient represents the true scene in the source image. Then, a Gaussian noise was added to the source images prior to fusion. The maximizing approach, the averaging approach, the LS approach, the window-based approach, and our two proposed approaches were used to fuse the three source images. The window-based approach assumes that the coefficients of source images within a $5 * 5$ window are constant and selects the coefficients which produce the highest energy of all pixels within that window. The intensity of the fused image is then estimated by (4). The whole process was

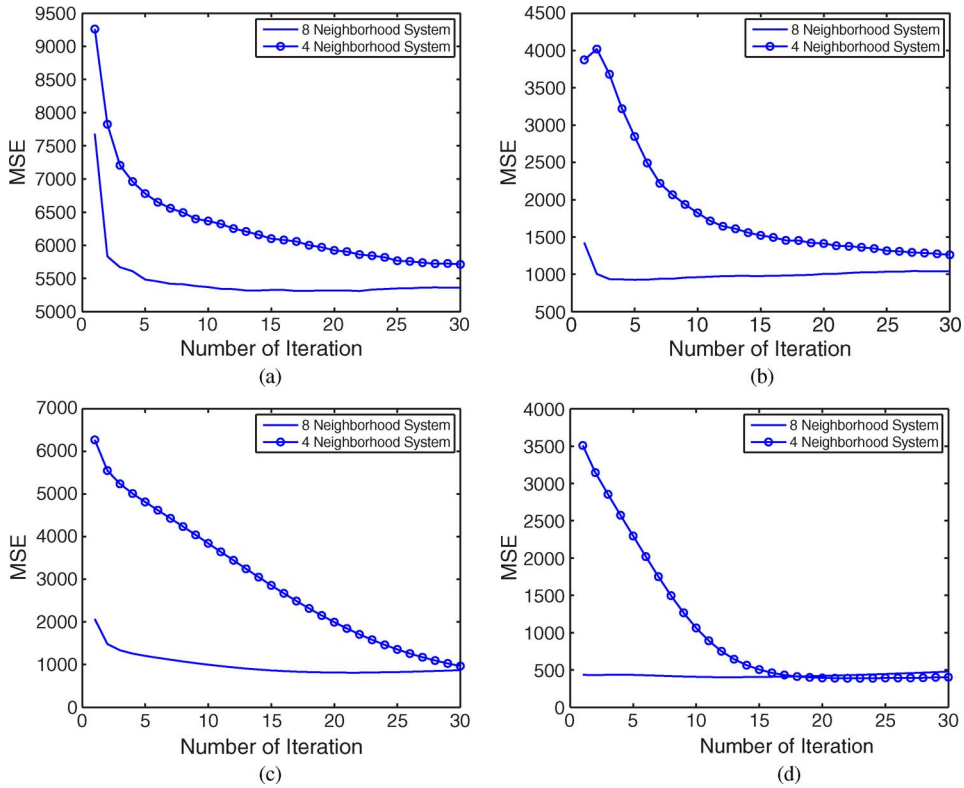

Fig. 3. MSE of fusion result as the number of iterations increases for MRF-based approaches for four- and eight-neighborhood systems. (a) MRF_H, SNR = 10 dB. (b) MRF_H, SNR = 30 dB. (c) MRF_HX, SNR = 10 dB. (d) MRF_HX, SNR = 30 dB.

repeated at two SNR levels, SNR = 10 dB and SNR = 30 dB. In addition to the visual inspection, we employed mean square error (mse) to evaluate the fusion performance in Experiment 1 in which a true reference scene is available. A smaller mse usually indicates a better fusion performance. The solid lines in Fig. 3 show the mse of fusion results using the MRF approaches with respect to the ground truth as the number of iterations increases. Initially, the coefficient mask and the fused image have much noise. As the number of iterations increases, the resulting coefficient mask and the fused image approach the ground truth and produce the smallest mse. We found that our new fusion algorithms converge after around three iterations at an SNR level of 30 dB and converge after around ten iterations at an SNR level of 10 dB.

MRF modeling is employed to include the dependences of decision making and/or pixel intensities of nearby pixels. The choice of neighborhoods affects the effectiveness of MRF modeling. Larger neighborhoods used in MRF modeling implies more spatial correlation in the image. In order to evaluate the fusion result for the different neighborhoods chosen, we also employed the four-neighborhood system, which only uses the three clique types C_1, C_2, and C_3 shown in Fig. 1 for MRF modeling, to compare with the fusion result using the eight-neighborhood system. The mses of fusion results using both neighborhood systems for MRF modeling are shown in Fig. 3. Although the algorithms using both neighborhood systems converge finally, it is observed that the MRF modeling using the eight-neighborhood system makes the algorithm converge faster than that for the four-neighborhood system. Furthermore, the use of the eight-neighborhood system produces a little smaller mse than that of the four-neighborhood system while using the algorithm MRF_H, while it produces a slightly larger mse with the algorithm MRF_HX. This observation implies that the use of a larger neighborhood system does not necessarily improve the performance and that the choice of different neighborhoods in MRF models does not impact much the final fusion result. We also note that the inclusion of more memory in the model results in improved performance, i.e., the eight-neighborhood system performs better than the four-neighborhood system.

Fig. 2 shows the three source images at an SNR level of 30 dB, and Fig. 4 shows the fusion results produced by the six fusion approaches, respectively. It is observed that the fused image produced by the algorithm MRF_HX displays reduced image noise at the cost of smoother image texture and is the closest to the ground truth. Fig. 5 shows the results for the estimated coefficients of the three source images using six fusion approaches. The window-based approach removed the noise quite effectively but produced a mosaic coefficient mask. The two MRF algorithms outperform the other four approaches and demonstrate good ability of accurately estimating the coefficients. Table I gives a quantitative comparison by means of the mse. We observed that the use of the spatial correlation property improves the fusion performance. Furthermore, the window-based approach and the algorithm MRF_H produce much smaller mses than the LS approach in the low SNR case, while they do not improve the performance much in the high SNR case. Our proposed fusion algorithm, MRF_HX, is observed to produce the smallest mse in both the low SNR case and the high SNR case. This also indicates that the estimation

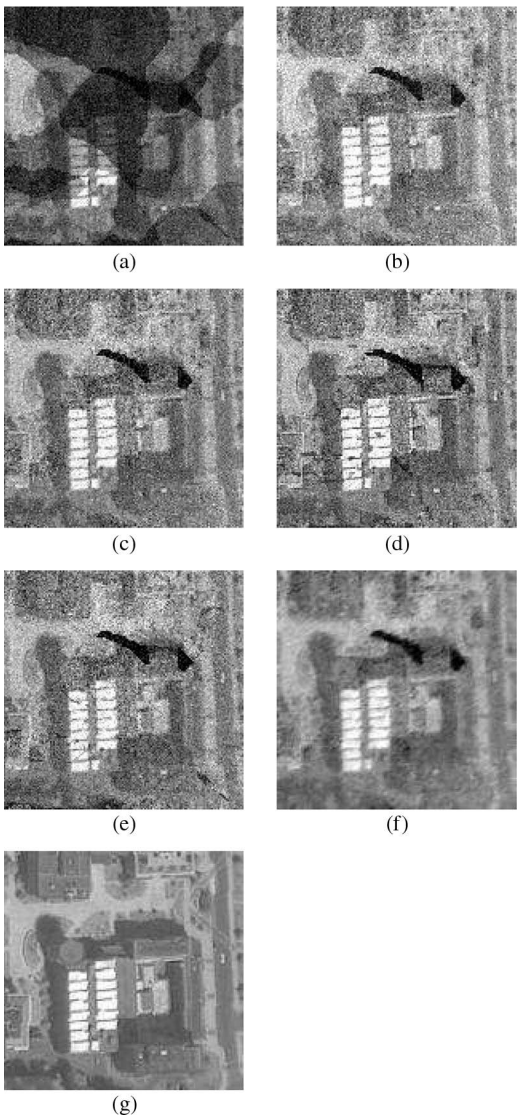

Fig. 4. Fusion results and true scene in experiment 1. (a) Averaging. (b) Maximizing. (c) LS. (d) Window. (e) MRF_H. (f) MRF_HX. (g) True scene.

accuracy of coefficients plays a much more important role in the fusion process in the low SNR case than that in the high SNR case.

Table II gives the execution times for the six fusion approaches. These six approaches are implemented using Matlab 7.1 and executed on a Computer with 4-G RAM and Intel Core2Quad CPU at 2.40 GHz. The two MRF-based approaches require relatively longer computational time than the other fusion approaches. However, the computation time can be easily reduced by dividing the whole image into several subimages and then processing the data in parallel.

2) Experiment 2—Real Data: In this experiment, we select three bands from a hyperspectral data set as the source images. Six fusion approaches are applied in this experiment to fuse the three source images. The three source images and the fusion results are shown in Figs. 6 and 7, respectively. Our model is a simplified model, and there is a certain mismatch between the model and the real image data set, e.g., the relationship between the source images and the true scene might not be explained simply by "contribute" or "not contribute" and the coefficient H_i can take on values other than $\{0, 1\}$. However, our algorithms still work quite well in practice. The results

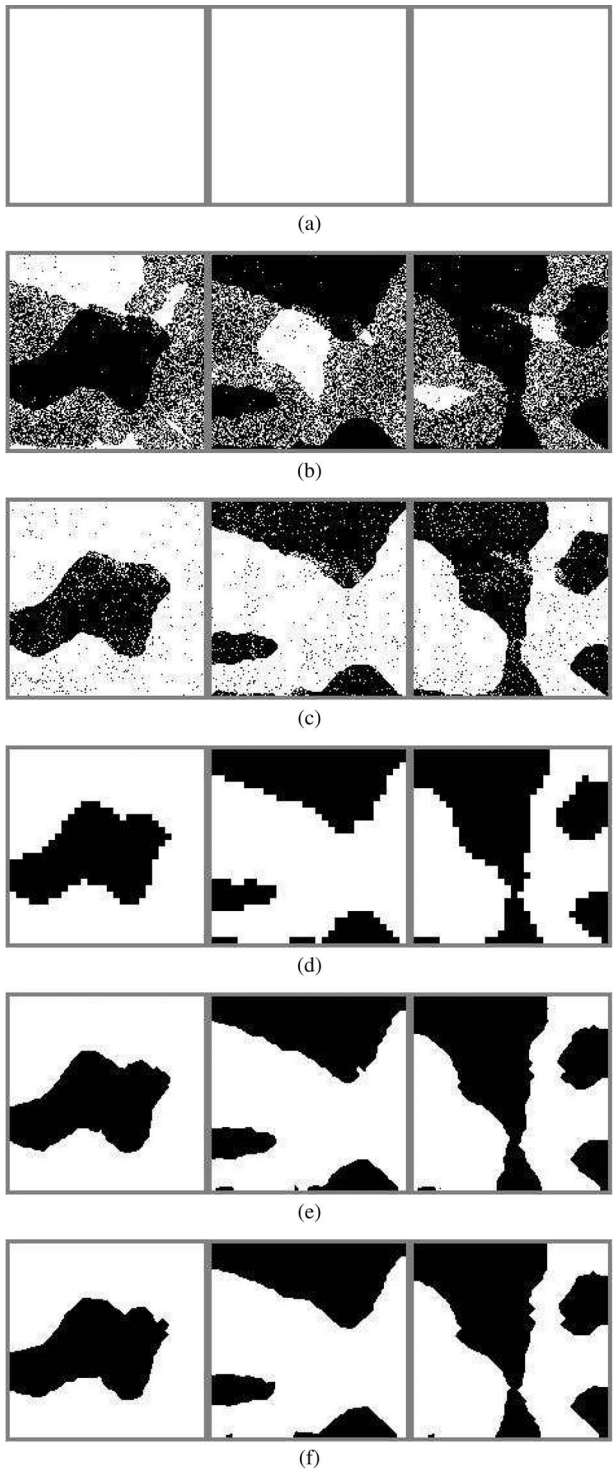

Fig. 5. Estimated coefficients of the three source images in Experiment 1. (a) Averaging. (b) Maximizing. (c) LS. (d) Window. (e) MRF_H. (f) MRF_HX.

TABLE I
MSE OF FUSION APPROACHES IN EXPERIMENT 1

SNR	Max	Ave	LS	Window	MRF_H	MRF_HX
10 dB	6490	6788	9174	6756	6316	3067
30 dB	1085	4425	877	862	851	496

TABLE II
EXECUTION TIME OF FUSION APPROACHES IN EXPERIMENT 1 (IN SECONDS)

Max	Ave	LS	Window	MRF_H	MRF_HX
0.0034	0.0022	4.76	5.26	31.52	43.87

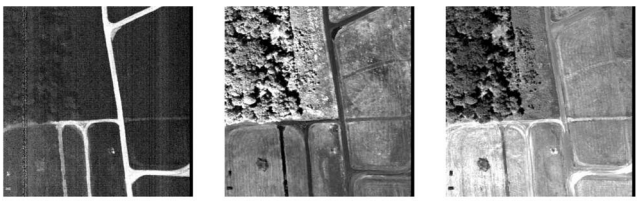

Fig. 6. Three source images in Experiments 2 and 3, size 155 $*$ 155. (a) Source 1. (b) Source 2. (c) Source 3.

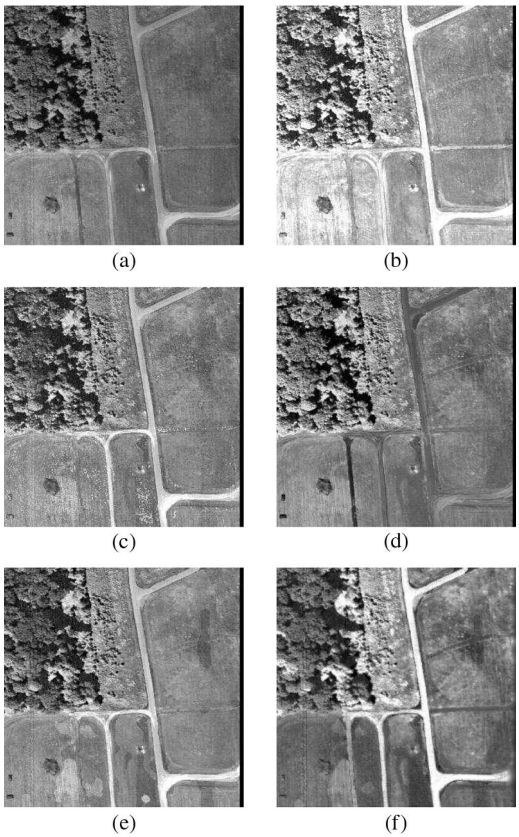

Fig. 7. Fusion results in Experiment 2, application with non-MD based fusion. (a) Averaging. (b) Maximizing. (c) LS. (d) Window. (e) MRF_H. (f) MRF_HX.

show that the use of the MRF model for both the coefficient and the fused image improves the fusion performance and enhances the image contrast. The fused images produced by the averaging approach and the window-based approach display low contrast. The LS approach produces more noise in the fused image. The fused image produced by the maximizing approach has high contrast, but it is too bright. It is observed that the algorithm MRF_HX produces the sharpest edges than the other approaches in the fused image and it preserves most textures.

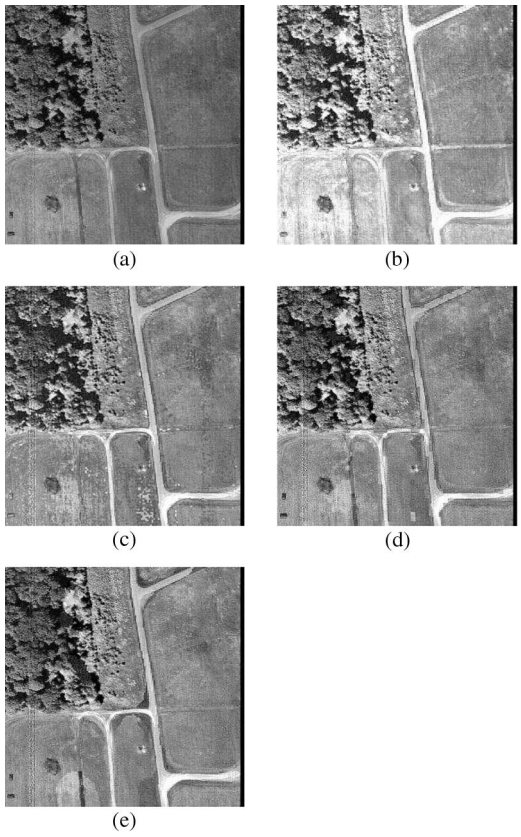

Fig. 8. Fusion results in Experiment 3, application with MD-based fusion. (a) Averaging. (b) Maximizing. (c) LS. (d) Window. (e) MRF_H.

D. Application With MD-Based Fusion

In the previous two experiments, we evaluated our two fusion algorithms for the non-MD based-fusion approach. In this section, we will evaluate the performance of algorithm MRF_H for the MD-based fusion approach. As discussed in Section III-C, due to the loss of the locality in the MRF models for the MD image representations, only the algorithm MRF_H is applied in the MD-based fusion approach.

1) Experiment 3: The three source images shown in Fig. 6 are also used in this experiment. Each source image is decomposed into four subimages by using the discrete 2-D Haar wavelet transform, and then, a fusion approach is employed to fuse the MD representations of the three source images at each level. Finally, the inverse Haar wavelet transform is computed from the fusion results at four levels. The maximizing approach, the averaging approach, the LS approach, the window-based approach, and the algorithm MRF_H are tested in the fusion process that involves wavelet representations. The fusion results are shown in Fig. 8. The maximizing approach still produces a fusion result that is too bright. The LS approach produces more noise in the fusion result. The fused image produced by the window-based approach displays a mosaic pattern. We observe that our algorithm MRF_H produces the most textures in the fused image. In addition, comparing Fig. 8(e) with Fig. 7(e), the MD-based fusion result produced by algorithm MRF_H [Fig. 8(e)] is observed to be closer to the source images with less artifacts. Note that a white spot, which does not appear in either of the three source images, is observed at the bottom

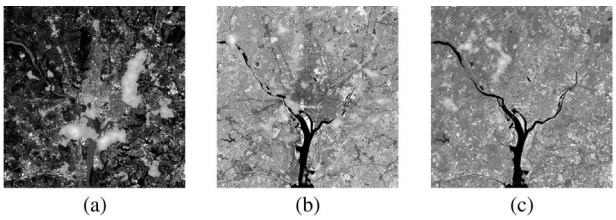

Fig. 9. Remotely sensed cloudy images used in Experiment 4. (a) Source 1. (b) Source 2. (c) Source 3.

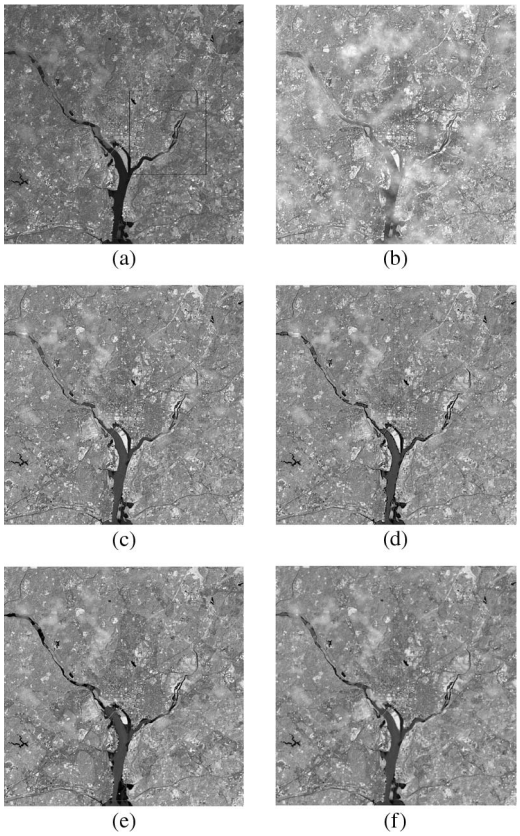

Fig. 10. Fusion results in Experiment 4—cloud images. (a) Averaging. (b) Maximizing. (c) LS. (d) Window. (e) MRF_H. (f) MRF_HX (non-MD-based approach).

of the non-MD-based fusion result produced by algorithm MRF_H [Fig. 7(e)] and the MD-based fusion result does not display such an artifact.

2) Experiment 4: As another example, three multispectral images are used to illustrate our algorithm and evaluate the fusion performance. Fig. 9 shows three bands from a multispectral data set downloaded from [35]. Artificial clouds have been added by Photoshop to the three images to create the occlusion. The multispectral images are from the Washington DC area, with size of $1020 * 1020$. This experiment tests the MD-based fusion performance for the cloud images. The same procedure for MD-based fusion, as described earlier, has been applied. The fusion results for five fusion approaches are shown in Fig. 10. The maximizing approach produces a fused result that is too bright. Fig. 11 shows the zoomed-in version of a boxed area of fused results for the other four approaches to more clearly examine the performance of the fusion algorithms.

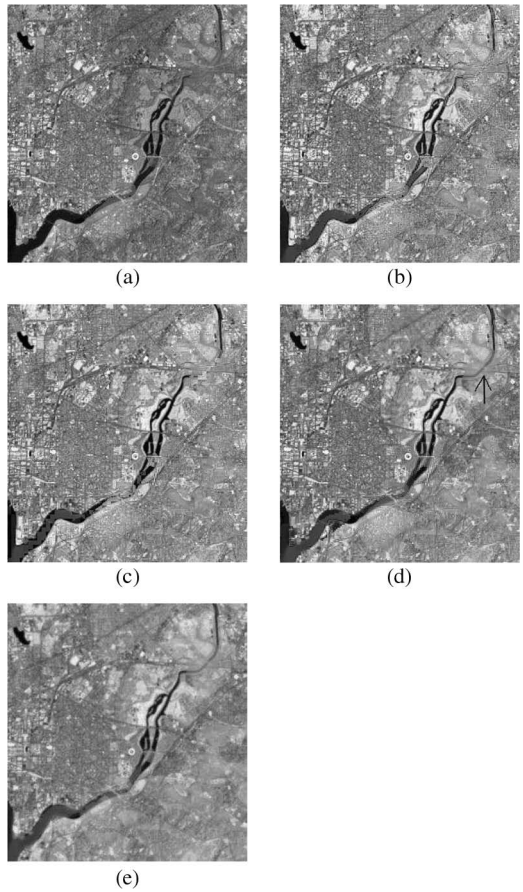

Fig. 11. Magnified fusion results in Experiment 4—cloud images. (a) Averaging. (b) LS. (c) Window. (d) MRF_H. (e) MRF_HX (non-MD-based approach).

We observe that our algorithm MRF_H produces the highest spatial resolution in the fused image and the fusion result contains less artifacts due to the cloud effect than the other approaches, which is marked with an arrow in Fig. 11(d). This experiment demonstrates the improvement in the performance of MD-based fusion approaches using MRF models. The MD-based approach is usually used for images with high resolution and when the computational cost is not a consideration. The non-MD-based approach is particularly useful for images with low resolutions and when the computational cost is a consideration. In this experiment, the fusion result using the MRF_HX algorithm with non-MD-based approach is also shown in Figs. 10(f) and 11(e). Compared with the MRF_H algorithm with MD-based approach, it is observed that the MD-based approach can eliminate the cloud effect more effectively than the non-MD-based approach and the MRF_HX algorithm can preserve more smooth edge information.

V. Conclusion

In this paper, we have studied the image fusion problem based on a statistical model. We utilized the fact that decision making in the fusion process has significant correlation within its neighborhood and assumed that it can be modeled as an MRF. Based on that, a new statistical fusion algorithm, namely, MRF_H, has been proposed. This approach is applicable for both non-MD- and MD-based fusion approaches. In particular,

when the raw source images are directly used for fusion without preprocessing, the fused image can also be modeled as an MRF, and then, the fusion result can be obtained using the MAP criterion incorporating the *a priori* Gibbs distribution of the fused image. The second algorithm, MRF_HX, is only applicable for non-MD-based fusion approaches. Visual inspection and quantitative performance evaluation both demonstrate that the employment of the MRF model in the fusion approaches resulted in a better fusion performance than the traditional fusion approaches. In our proposed image fusion algorithms, we assumed a simple relationship between each source image and the true scene, i.e., a source image either contributes to the fused image or does not contribute to the fused image. Thus, it results in a mismatch between the fusion model and the real image data set. To improve this, one can assume that the coefficient in the data model can take any real value, which may increase the accuracy of the fusion algorithms. In addition, in the developed image fusion algorithms, we assumed that the noise in the source image is an i.i.d. Gaussian noise. Since this is a rather limiting assumption, if we can build the noise model to include non-Gaussian distortion or possibly correlated Gaussian mixture distortion, this model should be closer to realistic sensor images and the estimation of fused image may improve.

REFERENCES

[1] R. S. Blum, "On multisensor image fusion performance limits from an estimation theory perspective," *Inf. Fusion*, vol. 7, no. 3, pp. 250–263, Sep. 2006.

[2] Z. Wang, D. Ziou, C. Armenakis, D. Li, and Q. Li, "A comparative analysis of image fusion methods," *IEEE Trans. Geosci. Remote Sens.*, vol. 43, no. 6, pp. 1391–1402, Jun. 2005.

[3] C. Thomas, T. Ranchin, L. Wald, and J. Chanussot, "Synthesis of multispectral images to high spatial resolution: A critical review of fusion methods based on remote sensing physics," *IEEE Trans. Geosci. Remote Sens.*, vol. 46, no. 5, pp. 1301–1312, May 2008.

[4] C. Pohl and J. van Genderen, "Multisensor image fusion in remote sensing: Concepts, methods, and applications," *Int. J. Remote Sens.*, vol. 19, no. 5, pp. 823–854, 1998.

[5] P. K. Varshney, B. Kumar, M. Xu, A. Drozd, and I. Kasperovich, "Image registration: A tutorial," in *Proc. NATO ASI*, Albena, Bulgaria, 2005.

[6] Z. Zhang and R. S. Blum, "A categorization of multiscale-decomposition-based image fusion schemes with a performance study for a digital camera application," *Proc. IEEE*, vol. 87, no. 8, pp. 1315–1326, Aug. 1999.

[7] R. K. Sharma, T. K. Leen, and M. Pavel, "Probabilistic image sensor fusion," in *Proc. Adv. Neural Inf. Process. Syst. 11*, 1999, pp. 824–830.

[8] H.-M. Chen, S. Lee, R. Rao, M.-A. Slamani, and P. Varshney, "Imaging for concealed weapon detection: A tutorial overview of development in imaging sensors and processing," *IEEE Signal Process. Mag.*, vol. 22, no. 2, pp. 52–61, Mar. 2005.

[9] Y. Zhang, S. De Backer, and P. Scheunders, "Noise-resistant wavelet-based Bayesian fusion of multispectral and hyperspectral images," *IEEE Trans. Geosci. Remote Sens.*, vol. 47, no. 11, pp. 3834–3843, Nov. 2009.

[10] P. Burt and R. Kolczynski, "Enhanced image capture through fusion," in *Proc. 4th Int. Conf. Comput. Vis.*, 1993, pp. 173–182.

[11] J. Yang and R. Blum, "A statistical signal processing approach to image fusion for concealed weapon detection," in *Proc. IEEE Int. Conf. Image Process.*, 2002, pp. 513–516.

[12] A. Lozci, A. Achim, D. Bull, and N. Canagarajah, "Statistical image fusion with generalized Gaussian and Alpha-Stable distributions," in *Proc. 15th Int. Conf. Digital Signal Process.*, 2007, pp. 268–271.

[13] E. Lallier and M. Farooq, "A real time pixel-level based image fusion via adaptive weight averaging," in *Proc. 3rd Int. Conf. Inf. Fusion*, 2000, pp. WEC3/3–WEC313.

[14] S. Z. Li, *Markov Random Field Modeling in Computer Vision*. New York: Spinger-Verlag, 2001.

[15] M. Joshi and A. Jalobeanu, "MAP estimation for multiresolution fusion in remotely sensed images using an IGMRF prior model," *IEEE Trans. Geosci. Remote Sens.*, vol. 48, no. 3, pp. 1245–1255, Mar. 2010.

[16] T. Kasetkasem and P. Varshney, "An image change detection algorithm based on Markov random field models," *IEEE Trans. Geosci. Remote Sens.*, vol. 40, no. 8, pp. 1815–1823, Aug. 2002.

[17] Z. Tu and S. Zhu, "Image segmentation by data-driven Markov chain Monte Carlo," *IEEE Trans. Pattern Anal. Mach. Intell.*, vol. 24, no. 5, pp. 657–673, May 2002.

[18] H. Chen, "Mutual information based image registration with applications," Ph.D. dissertation, Syracuse Univ., Syracuse, NY, May, 2002.

[19] S. Geman and D. Geman, "Stochastic relaxation, Gibbs distributions, and the Bayesian restoration of images," in *Readings in Uncertain Reasoning*. San Francisco, CA: Morgan Kaufmann, 1990, pp. 452–472.

[20] L. Bedini, A. Tonazzini, and S. Minutoli, "Unsupervised edge-preserving image restoration via a saddle point approximation," *Image Vis. Comput.*, vol. 17, no. 11, pp. 779–793, Sep. 1999.

[21] D. Kundur, D. Hatzinakos, and H. Leung, "Robust classification of blurred imagery," *IEEE Trans. Image Process.*, vol. 9, no. 2, pp. 243–255, Feb. 2000.

[22] W. Wright, "Fast image fusion with a Markov random field," in *Proc. 7th Int. Conf. Image Process. Appl.*, 1999, pp. 557–561.

[23] R. S. Blum, "Robust image fusion using a statistical signal processing approach," *Inf. Fusion*, vol. 6, no. 2, pp. 119–128, Jun. 2005.

[24] S. M. Kay, *Fundamentals of Statistical Signal Processing: Estimation Theory*. Upper Saddle River, NJ: Prentice-Hall, 1993.

[25] Y. C. Eldar, A. Beck, and M. Teboulle, "Bounded error estimation: A Chebyshev center approach," in *Proc. 2nd IEEE Int. Workshop Comput. Adv. Multi-Sensor Adapt. Process.*, 2007, pp. 205–208.

[26] S. Lakshmanan and H. Derin, "Simultaneous parameter estimation and segmentation of Gibbs random fields using simulated annealing," *IEEE Trans. Pattern Anal. Mach. Intell.*, vol. 11, no. 8, pp. 799–813, Aug. 1989.

[27] V. Kolmogorov and R. Zabin, "What energy functions can be minimized via graph cuts?" *IEEE Trans. Pattern Anal. Mach. Intell.*, vol. 26, no. 2, pp. 147–159, Feb. 2004.

[28] F. Heitz, "Restriction of a Markov random field on a graph and multiresolution statistical image modeling," *IEEE Trans. Inf. Theory*, vol. 42, no. 1, pp. 180–190, Jan. 1996.

[29] P. Bremaud, *Markov Chains, Gibbs Fields, Monte Carlo Simulation, and Queues*. New York: Springer-Verlag, 1999.

[30] H. Derin and H. Elliott, "Modeling and segmentation of noisy and textured images using Gibbs random fields," *IEEE Trans. Pattern Anal. Mach. Intell.*, vol. PAMI-9, no. 1, pp. 39–55, Jan. 1987.

[31] T. Kasetkasem, "Image analysis methods based on Markov random field models," Ph.D. dissertation, Syracuse Univ., Syracuse, NY, Dec., 2002.

[32] S. S. Saquib, C. A. Bouman, and K. Sauer, "ML parameter estimation for Markov random fields, with applications to Bayesian tomography," *IEEE Trans. Image Process.*, vol. 7, no. 7, pp. 1029–1044, Jul. 1998.

[33] J. Besag, "On the statistical analysis of dirty pictures," *J. R. Stat. Soc.*, vol. 48, no. 3, pp. 259–302, 1986.

[34] S. Geman and C. Graffigne, "Markov random field image models and their application to computer vision," in *Proc. Int. Congr. Mathematicians*, 1986, pp. 1496–1517.

[35] R. C. Gonzalez and R. E. Woods, *Digital Image Processing*. Upper Saddle River, NJ: Prentice-Hall, 2008.

Min Xu (S'07–M'10) received the B.S. degree from the University of Science and Technology of China, Hefei, China, in 2002 and the M.S. and Ph.D. degrees in electrical engineering from Syracuse University, Syracuse, NY, in 2005 and 2009, respectively.

Since December 2009, she has been a Researcher with Blue Highway, LLC, Syracuse. Her research interests are in the areas of statistical signal and image processing.

Hao Chen (S'06–M'08) received the Ph.D. degree in electrical engineering from Syracuse University, Syracuse, NY, in 2007.

In 2007–2010, he was a Postdoctoral Research Associate and then a Research Assistant Professor with Syracuse University. Since August 2010, he has been an Assistant Professor with the Department of Electrical and Computer Engineering, Boise State University, Boise, ID. His research interests include statistical signal and image processing and communications.

Pramod K. Varshney (S'72–M'77–SM'82–F'97) received the B.S. degree in electrical engineering and computer science and the M.S. and Ph.D. degrees in electrical engineering from the University of Illinois at Urbana–Champaign, Urbana, in 1972, 1974, and 1976, respectively.

Since 1976, he has been with Syracuse University, Syracuse, NY, where he is currently a Distinguished Professor of Electrical Engineering and Computer Science and the Director of The Center for Advanced Systems and Engineering. His current research interests are in distributed sensor networks and data fusion, detection and estimation theory, wireless communications, image processing, radar signal processing, and remote sensing.

Dr. Varshney has received numerous awards. He serves as a Distinguished Lecturer for the IEEE Aerospace and Electronic Systems Society. He was the 2001 President of the International Society of Information Fusion.